Talanta 85 (2011) 2534–2541

Contents lists available at ScienceDirect

Talanta

journal homepage: www.elsevier.com/locate/talanta

Kinetic study of a complex triangular reaction system in alkaline aqueous-ethanol medium using on-line transmission FTIR spectroscopy and BTEM analysis

Martin Tjahjono*, XiuRong Li, FengLin Tang, Kanicha Sa-ei, Marc Garland*

*Institute of Chemical and Engineering Sciences, Agency for Science, Technology and Research (A*STAR), 1 Pesek Road, Jurong Island, Singapore 627833, Singapore*

ARTICLE INFO

Article history:
Received 27 June 2011
Received in revised form 4 August 2011
Accepted 5 August 2011
Available online 12 August 2011

Keywords:
On-line reaction monitoring
Multivariate analysis
Solvent effect
Spectral deconvolution

ABSTRACT

The kinetics of the base-catalyzed reaction of methyl 4-hydroxybenzoate in aqueous-ethanol solvent medium was studied and analyzed via combined on-line transmission FTIR spectroscopy and Band-Target Entropy Minimization (BTEM) technique. This reaction is considered complex since it involves simultaneous hydrolysis and ethanolysis reactions of methyl 4-hydrozybenzoate (MP) to form ethyl 4-hydroxybenzoate (EP) as an intermediate and sodium 4-hydroxybenzoate as a final product. The pure component spectra of the reactive species involved in the reaction were reconstructed using BTEM technique. Their corresponding real concentrations were calculated and subsequently used for analyzing the kinetics of this triangular reaction system. The effects of temperature and solvent mixture compositions were studied. In general, the results show that the rates of both hydrolysis and ethanolysis reactions increase with temperature. Addition of ethanol to the solvent mixture also reduces the rates of the hydrolysis reactions. The effect of solvent mixture on the rate of ethanolysis reaction is more complex and influenced by at least two competing factors, namely the concentration of ethoxide ion in the solution and the stabilization effect on the reactant. The enthalpy and entropy activation parameters, $\Delta H^{\ddagger}$ and $\Delta S^{\ddagger}$, of both the hydrolysis and ethanolysis reactions were determined using the Eyring equation and the activation parameters confirm the associative nature in the elementary steps in these reactions. Finally, it is shown that the dominant synthetic pathway in this triangular system changes from direct hydrolysis of methyl 4-hydrozybenzoate to the indirect pathway via ethanolysis and then hydrolysis depending on the solvent mixture composition.

1. Introduction

A wide variety of complex organic reactions have been successfully carried out in aqueous and mixed aqueous–organic solvents [1–5]. These reactions include, but are not restricted to, alkylations, carbonylations, metathesis, hydroformylation, etc. Fundamental information on the reaction kinetics is indispensible when the chemical syntheses are to be performed on a larger scale. A detailed kinetic investigation is essential not only to better understand the reaction mechanism, but also to assess the optimum reaction conditions, to achieve desirable product distribution, yield and selectivity and to facilitate reactor designs. Many chemical syntheses are quite complex and may consist of several parallel and/or sequential steps involving various intermediates. Reliable analytical techniques to accurately monitor complex organic reactions are undoubtedly important to achieve desired yield and selectivity patterns and hence develop a greener synthetic process.

A number of in situ or on-line spectroscopic techniques have played a significant role for investigating complex reactions by providing accurate understanding of speciation as well as kinetic and mechanistic information [6–9]. Pioneering work using infrared spectroscopy was largely directed toward better understanding organometallic chemistry [10–15] and homogeneously catalyzed organic syntheses of industrial interest [16–19]. Pioneering work using NMR was also directed toward organometallic chemistry [20–22] and homogeneously catalyzed organic syntheses [23,24]. In the last decade, in situ Raman measurements of organic syntheses have been reported [25–28]. Another noteworthy development has been the combined application of in situ spectroscopic techniques together with advanced signal processing techniques in order to analyze the highly over-lapping spectra from complex chemical reactions. In this regard, Band-Target Entropy Minimization (BTEM) [29–31] has been extensively used to identify the presence of reactive intermediates at trace levels in organic media [32–34].

In spite of its considerable potential, the utility of combined spectroscopic and signal processing techniques for investigating complex organic reactions carried out in aqueous and mixed aqueous–organic solvent media has not been extensively explored.

* Corresponding authors. Tel.: +65 6796 3960; fax: +65 6316 6185.
E-mail addresses: martin_tjahjono@ices.a-star.edu.sg (M. Tjahjono), marc_garland@ices.a-star.edu.sg (M. Garland).

0039-9140/$ – see front matter © 2011 Elsevier B.V. All rights reserved.
doi:10.1016/j.talanta.2011.08.016

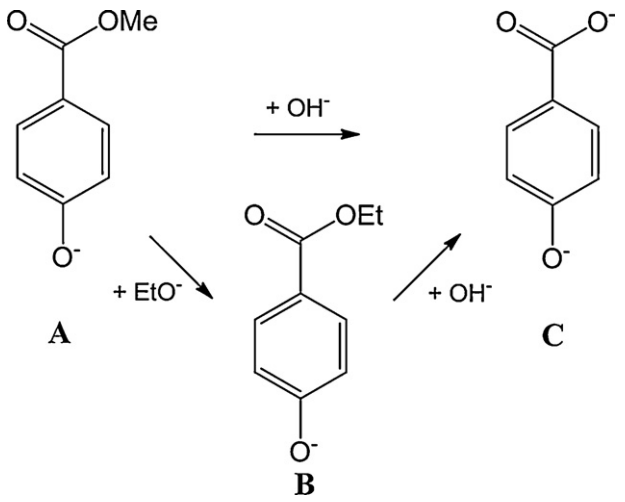

Scheme 1. Triangular reaction system – simultaneous hydrolysis and ethanolysis of MP (deprotonated) in alkaline aqueous-ethanol media.

More specifically, transmission FTIR spectroscopy is a relatively less utilized method [35–37] as compared to Raman and ATR-FTIR spectroscopy for monitoring reactions in aqueous or aqueous–organic solvents. This is largely due to the strong absorptivity of water over most of the mid-infrared range. However, it should be noted that spectra produced by transmission FTIR spectroscopy frequently have higher sensitivity than those of Raman spectra. In contrast to ATR spectra which possess some peak shifts and intensity differences [38], the spectra obtained from transmission FTIR are more readily interpreted and the quantitative analyses using transmission spectra are not hindered due to the non-linear optical effects associated with the absorption–reflection nature [39].

In this contribution, the utility of on-line transmission FTIR spectroscopy and an advanced spectral data processing, Band-Target Entropy Minimization (BTEM) is demonstrated to investigate the kinetics of a triangular complex reaction performed in mixed aqueous–organic solvent. A triangular reaction system is chosen in this study since it represents an archetypical complex reaction system which has been subject of considerable theoretical study [40,41]. Some well-known examples of reactions following the triangular model reaction system are (i) isomerization of 1-butene [42] and (ii) methanol formation from simultaneous CO and CO_2 [43,44].

In this study, the triangular reaction system is shown by the simultaneous hydrolysis and ethanolysis of methyl 4-hydrozybenzoate or methyl paraben (MP) (deprotonated form, **A**) carried out in alkaline aqueous-ethanol solvent media (see Scheme 1) [45]. The ethanolysis reaction involves the formation of intermediate **B** before it is finally transformed into product **C**. The kinetic rates of these complex reactions are analyzed using the quantitative information provided by the combined on-line FTIR transmission spectroscopy and BTEM. Kinetic study of this reaction is particularly interesting since the reactant MP has been widely used as preservatives in foods, drugs, cosmetics and beverages, etc. [46]. The reactions are also carried out at different temperatures and with different solvent mixture compositions to understand these effects on the transformation rates for each individual step of reaction. The kinetic results achieved by the combined in situ spectroscopic and signal processing techniques are ultimately used to ascertain the primary synthetic pathway in the complex triangular reaction system.

In summary, the present contribution demonstrates that qualitative (speciation) and quantitative information can be obtained from combined transmission FTIR and spectral data analysis for complex aqueous-phase organic syntheses. Subsequently, and depending on the system under study, the obtained kinetic parameter estimation can be further used to optimize the reaction. For example it might be possible due to the insight gained, to judiciously select reactions conditions where more environmentally friendly solvent mixture compositions can be used (thus lowering the effluent loading factor), or where better selectivity patterns or better conversion can be achieved.

2. Experimental

2.1. Materials

Methyl 4-hydroxybenzoate or methyl paraben (MP) (Sigma–Aldrich, Sigma Ultra, 99%+) and sodium hydroxide pellets (Merck, pro analysis, >99%) were used directly without further purification. The purity of the substrate MP was checked by ^{1}H NMR after dissolution in $CDCl_3$ (Bruker Avance 400 MHz with 0.5 WB, equipped with a 5 mm TBI probe with *z* gradient, running a standard Bruker supplied pulse sequence). These measurements indicated only very minor levels of impurities. Integration of the proton resonances provided lower bounds for the purity of MP (>99.5%). Solvent mixtures were prepared by mixing ethanol (VMR International Ltd, HPLC grade, 99.7–100%, v/v) with de-ionized ultra pure water (Young Lin Instrument, Aquamax™ – Basic 321 Water Purification System). In addition, ethyl 4-hydroxybenzoate or ethyl paraben (EP) (Alfa Aesar, 99%) and sodium 4-hydroxybenzoate (Sigma–Aldrich) were also used in this study to confirm the pure component spectra of the intermediate and the product of the reaction.

2.2. Equipment

The experimental setup consisted of a 50 mL glass jacketed reactor equipped with a magnetic stirrer, a Teflon membrane pump (Cole-Parmer), and a flow-through IR transmission cell. The temperature of the reactor was kept isothermal using a temperature bath circulator (Polyscience 9105, with temperature stability ± 0.05 K). The liquid was pumped in a closed looped from the reactor through the pump to the infrared flow-through cell and recycled back to the reactor.

Mid-infrared spectra were collected using a mid-infrared Equinox 55 FTIR Bruker spectrometer. The CaF_2 single crystal windows used (Korth Monokristalle, Kiel, Germany,) had dimensions of diameter 20 mm by thickness 2 mm. Two sets of Viton gaskets provided sealing and Teflon spacers (thickness of 25 μm) were used between the windows. Purified dry air was used to purge the spectrometer.

2.3. Reaction kinetic experiments

The reaction was carried out in alkaline water–ethanol solvent mixtures (circa 0.0125 mol of sodium hydroxide in 25 mL total solvent). Water, ethanol and sodium hydroxide were added sequentially into the reactor with stirring rate of circa 400 rpm. At each step, the liquid was thoroughly mixed and circulated through the infrared cell in order to measure the infrared spectra of water, water + ethanol, and water + ethanol + sodium hydroxide, respectively. Water and ethanol were introduced into the reactor using a syringe. The respective amounts were determined by weighing the syringe before and after injection using a balance (GR-200, A&D, Japan) with a precision of $\pm 10^{-4}$ g. The masses of sodium hydroxide pellets and reactant MP were determined directly using the same balance.

Table 1
Summary of the experimental runs performed in the study.

Exp Run	T (°C)	%(v/v) water–EtOH	Water (g)	EtOH (g)	NaOH (g)	MP (g)
Reproducibility						
1	25	86	21.615	2.839	0.475	0.189
2	25	86	21.417	2.720	0.483	0.188
3	25	86	21.482	2.789	0.478	0.189
Temperature variations						
4	15	86	21.455	2.801	0.483	0.189
5	20	86	21.522	2.782	0.493	0.190
6	30	86	21.461	2.777	0.490	0.189
7	35	86	21.518	2.805	0.488	0.188
Solvent mixture variations						
8	35	70	17.546	5.972	0.480	0.189
9	35	50	12.523	9.710	0.483	0.188
10	20	70	17.489	5.922	0.487	0.189
11	20	50	12.541	9.756	0.485	0.188

The reactions started immediately upon introduction of reactant MP into the reactor. The dissolution of solid MP occurred in less than 30 s. The infrared spectra of the solution in the range 1080–1550 cm^{-1} (with resolution of 2 cm^{-1} and 16 co-added scans) were recorded automatically every 300 s or 120 s (in experiments at T = 35 °C) to monitor the course of reactions.

A total of 11 experimental runs were conducted at various conditions (i.e. different temperatures and solvent mixture compositions). Replicates of the experimental runs were also performed in order to confirm the reproducibility of the kinetic measurements. Experimental details on various runs are summarized in Table 2. An experimental reaction temperature of 25 °C was chosen to validate the reproducibility of experiments. The solvent mixture composition at 86% (v/v) water–ethanol was chosen to study the effect of temperature (Table 1).

Additionally, GC–MS and NMR measurements were carried out in order to confirm the presence the three reactive species observed in the reactions. The GC–MS analysis on the reaction solution confirmed that the reaction proceeded to completion, and there were no additional side products. The NMR analysis confirmed the identity of the final product **C** (sodium paraben).

Table 2
Summary of the second-order rate constants k_1, k_2 and k_3 (in l mol^{-1} s^{-1}) for all experimental runs. These rate constants are corresponding to the hydrolysis reaction of the deprotonated MP (Eq. (6)), the hydrolysis reaction of the deprotonated EP (intermediate) (Eq. (7)), and the ethanolysis of the deprotonated MP (Eq. (8)), respectively.[a]

Exp Run	T (°C)	%(v/v) water–EtOH	$k_1 \times 10^4$	$k_2 \times 10^4$	$k_3 \times 10^4$
Reproducibility					
1	25	86	4.49	1.63	35.1
2	25	86	4.84	1.83	37.4
3	25	86	4.68	1.66	35.1
Average			4.67 ± 0.18	1.71 ± 0.11	35.8 ± 0.13
Temperature variations					
4	15	86	2.83	1.06	25.0
5	20	86	3.67	1.03	25.1
6	30	86	5.95	2.60	56.4
7	35	86	7.52	2.97	62.8
Solvent mixture variations					
8	35	70	3.41	1.16	17.4
9	35	50	0.83	0.11	10.3
10	20	70	1.64	0.45	8.90
11[b]	20	50	0.33	0.10	3.16

[a] In the present analysis, the period of the first 20,000 s of the reaction time was selected for performing kinetic analysis. This time frame could provide sufficient information related to the change of concentrations for all the reactant, the intermediate and the product which are required for the kinetic analysis.

[b] Calculated using a longer time frame (the first 40,000 s reaction time) since the reactions at this experimental condition are relatively slow.

3. Numerical aspects

The data analyses for this kinetic study were partitioned into three main steps, (1) spectroscopic data processing and deconvolution of the pure component spectra, (2) determination of concentrations and (3) evaluation of the kinetic rate constants. These three steps are described in detail in the following sections.

3.1. Spectroscopic data processing and deconvolution of pure component spectra

The infrared spectra of water, water + ethanol, and water + ethanol + sodium hydroxide were measured sequentially before the reaction started. The pure component spectra of water, ethanol, and 'sodium hydroxide' were obtained using optimal subtraction procedures [47]. It should be noted that the spectrum of 'sodium hydroxide' included the spectral contribution of the combined ethoxide and hydroxide ions which are present in equilibrium in solution (see more details in the later section).

Singular value decomposition (SVD) and thereafter BTEM analysis [29–31] were performed on the raw reaction spectra to obtain the normalized pure component spectra of the reactive species (i.e. reactant **A**, intermediate **B** and product **C**, see Scheme 1). Only circa 10–15 significant transposed right singular vectors (obtained form SVD) were used in order to reconstruct the pure component spectra of these reactive species.

The raw reaction spectra were subsequently treated in order to subtract the spectral contributions from the background (moisture), solvents (water and ethanol) and 'sodium hydroxide' as well as to correct the slight baseline shifts using a baseline correction procedure [48]. These preprocessed spectra were denoted as $\mathbf{A}_{k\times v}$ and subsequently used to analyze the concentrations of the 3 reactive species shown in Scheme 1.

3.2. Determination of concentrations

Infrared absorbance spectra can be modeled by the empirical Lambert–Beer–Bouguer law (Eq. (1)), where $\mathbf{A}_{k\times v}$, $\mathbf{C}_{k\times s}$, $\hat{\mathbf{a}}_{s\times v}$, and $\mathbf{d}_{s\times s}$ are the absorbance spectra, the concentration of the reactive species, the normalized pure component absorptivities (from BTEM analysis) and the scaling elements which accounts for both the path length and molar absorptivities of each species, respectively. The subscripts k and v denote the number of spectra in one experimental run and the number of data channels associated with the spectroscopic wavenumber range.

$$\mathbf{A}_{k\times v} = \mathbf{C}_{k\times s}\mathbf{d}_{s\times s}\hat{\mathbf{a}}_{s\times v} \tag{1}$$

Concentrations of these species can be estimated from (Eq. (2)) where $[\hat{\mathbf{a}}_{s\times v}]^+$ is the pseudo inverse matrix of $\hat{\mathbf{a}}_{s\times v}$. Proper scaling elements $\mathbf{d}_{s\times s}$ must be evaluated in order to evaluate the concentrations.

$$\mathbf{C}_{k\times s} = \mathbf{A}_{k\times v}[\hat{\boldsymbol{a}}_{s\times v}]^+(\mathbf{d}_{s\times s})^{-1} \tag{2}$$

Since only three major reactive species (i.e. s = 3) are involved in this reaction, namely reactant **A**, intermediate **B**, and product **C**, and since the reaction was carried out in a closed system, the total concentration of **A** + **B** + **C** at any reaction time are conserved and should be equal to the initial concentration of MP used in each experimental run $\mathbf{C}^{\mathbf{o}}_{k1}$ (Eq. (3)). In this analysis, it assumes that the volume changes due to reactions in this concentration range are negligible.

$$\text{Minimize}\quad \mathbf{G} = \sum_{k}\left(\mathbf{C}^{\mathbf{o}}_{k1} - \sum_{s=1,2,3}\mathbf{C}_{ks}\right)^2 \tag{3}$$
$$w.r.t\ \mathbf{d}_{3\times 3}$$

Using a least square minimization procedure, the scaling elements $\mathbf{d}_{3\times3}$ were obtained and the concentrations of each species as a function of reaction time can be subsequently determined (Eq. (2)).

3.3. Reaction chemistry

The reactive system is rather complex and can be described by 3 sets of equilibria and elementary steps [45].

(i) the rapid equilibrium between ethanol, hydroxide ion, ethoxide ion and water [19]:

$$EtOH + OH^- \leftrightharpoons EtO^- + H_2O \quad (4)$$

(ii) the very fast deprotonation of MP upon dissolution (nearly instantaneous):

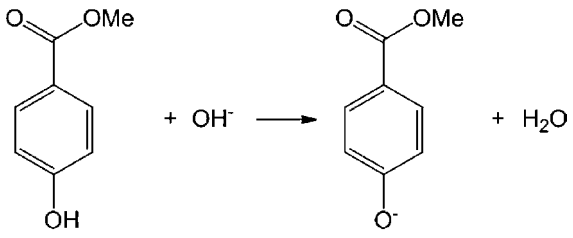

A (5)

(iii) simultaneous hydrolysis and ethanolysis reactions with rate constants k_i (see Scheme 1):

$$\mathbf{A} + OH^- \xrightarrow{k_1} \mathbf{C} + MeOH \quad (6)$$

$$\mathbf{B} + OH^- \xrightarrow{k_2} \mathbf{C} + EtOH \quad (7)$$

$$\mathbf{A} + EtO^- \xrightarrow{k_3} \mathbf{B} + MeO^- \quad (8)$$

It should be noted that since the concentration of methoxide ion in solution is much less than ethoxide ion in solution i.e. $([MeOH]:[EtOH])_{max} < 0.02$, the reversed reaction of Eq. (8) can be simply neglected.

3.4. Evaluation of rate constants

The rate of change in the concentrations of reactant **A**, intermediate **B** and product **C** can be written as Eqs. (9)–(11), respectively.

$$\frac{dC_{\mathbf{A}}}{dt} = -k_1 C_{\mathbf{A}} C_{OH^-} - k_3 C_{\mathbf{A}} C_{EtO^-} \quad (9)$$

$$\frac{dC_{\mathbf{B}}}{dt} = -k_2 C_{\mathbf{B}} C_{OH^-} + k_3 C_{\mathbf{A}} C_{EtO^-} \quad (10)$$

$$\frac{dC_{\mathbf{C}}}{dt} = (k_1 C_{\mathbf{A}} + k_2 C_{\mathbf{B}}) C_{OH^-} \quad (11)$$

Since the concentrations of hydroxide ion C_{OH^-} and ethoxide ion C_{EtO^-} in solution are equilibrated (see Eq. (4)), they are related by an equilibrium constant K as shown in Eq. (12). The corresponding equilibrium constant as a function of temperature has been previously reported [45,49,50] and can be directly used in this study. The mass balance for the hydroxide ion concentration in the solution is given by Eq. (13), where $C^o_{OH^-}$ and C^o_{MP} are the initial concentrations of hydroxide ion and MP, respectively. The concentration of ethanol C_{EtOH} is calculated from the initial concentration C^o_{EtOH} and the amount of ethanol consumed for the equilibrium reaction (Eq. (4)). The concentration of water C_{H_2O} (Eq. (15)) is assumed constant during reaction (equal to its initial concentration $C^o_{H_2O}$), as water is used in circa 50–100 fold excess compared to $C^o_{OH^-}$.

$$C_{EtO^-} = \frac{K C_{OH^-} C_{EtOH}}{C_{H_2O}} \quad (12)$$

$$C_{OH^-} = C^o_{OH^-} - C^o_{MP} - C_{\mathbf{C}} - C_{EtO^-} \quad (13)$$

$$C_{EtOH} = C^o_{EtOH} - C_{EtO^-} \quad (14)$$

$$C_{H_2O} \approx C^o_{H_2O} \quad (15)$$

The concentrations of the reactive species obtained from the spectroscopic analysis (Section 3.2) were utilized accordingly in order to evaluate the second-order rate constants of the hydrolysis and ethanolysis reactions. Numerical integration using 4th order Runge Kutta combined with the iteration procedure were employed to solve a set of ordinary differential equations shown in Eqs. (9)–(11) involving the equilibrium equation (Eq. (12)). The iteration calculations were performed until the concentrations obtained from numerical calculations converged to the concentrations obtained from the spectroscopic analysis.

All the numerical analyses described above (spectral subtraction, BTEM analysis, evaluations of concentrations and rate constants) were performed in MATLAB (v. R2007b).

4. Results and discussion

4.1. Infrared spectroscopic analysis

Since solvent water and ethanol have strong bands at around 1650 cm^{-1} and 1050 cm^{-1}, the wavenumber range in between at 1080 and 1550 cm^{-1} was selected for quantitative analysis. This avoids various complications associated with these two strong bands. The CaF_2 windows used in this study have a strong cut-off at circa 1000 cm^{-1} which is outside of the spectral range used for analysis.

The typical raw reaction spectra in the wavenumber range 1080–1550 cm^{-1} and their preprocessed spectra are shown in Fig. 1(a) and (b), respectively. The latter was obtained by subtracting the spectral contributions of water, ethanol, and 'sodium hydroxide' as well as background (moisture) from the raw spectra. The baseline correction procedure was also applied to account for the baseline shifts. The preprocessed spectra are herein denoted as $\mathbf{A}_{k\times\nu}$. These spectra are subsequently used for all further quantitative analysis.

The preprocessed reaction spectra in Fig. 1(b) contain the spectral contributions of the major reactive species. BTEM analysis was employed in order to identify and reconstruct the underlying pure component spectra of the reactive species. It should be noted that the reaction spectra were quite sensitive to the solvent composition of water and ethanol used, while the reaction spectra were far less sensitive to variations in temperature. Accordingly, BTEM analyses were carried out on 3 sets of spectra, obtained from Exp Run {1–7}, {8,10} and {9,11}.

The bands at circa 1288, 1284 and 1378 cm^{-1} observed in the right singular vectors were chosen as targets for the BTEM analysis. These target bands successfully resulted in three different pure component spectra as shown in Fig. 2(a)–(c). These pure component spectra can be assigned to the reactant **A** (deprotonation of MP), the intermediate **B** (deprotonation of EP) and the product **C** (sodium paraben), respectively. The pure component spectra of intermediate **B** and product **C** are consistent with the spectra of ethyl 4-hydroxybenzoate and sodium 4-hydroxybenzoate dissolved in alkaline water–ethanol mixture, respectively. These three pure component spectra can also be compared to those pure component spectra previously reported for a combined spectroscopic

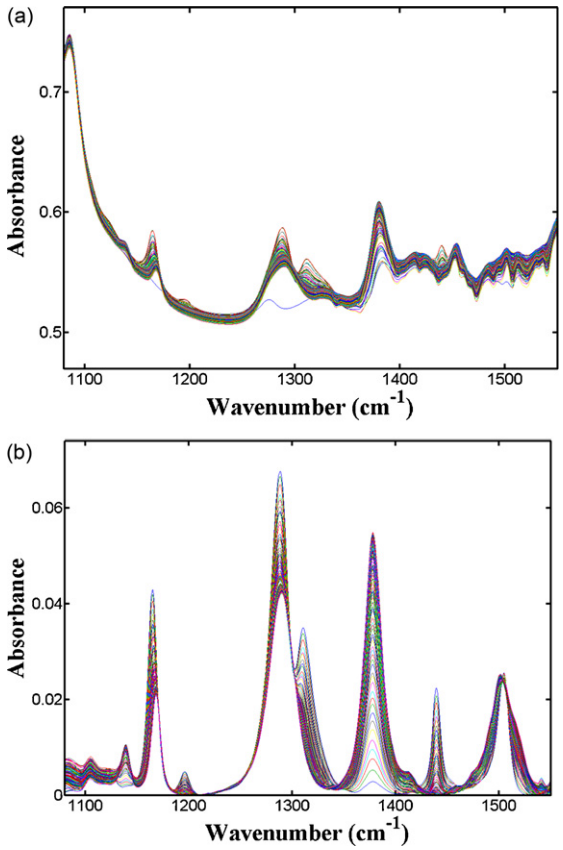

Fig. 1. (a) The raw infrared reaction spectra and (b) the preprocessed spectra of the simultaneous hydrolysis and ethanolysis of deprotonated MP in alkaline water–ethanol solvent media (measured in Exp Run 1).

and calorimetric investigation on a parallel hydrolysis reaction scheme [37].

The pure component spectrum of reactant **A** (deprotonation of MP) is somewhat similar to that of intermediate **B** (deprotonation of EP). Both spectra show strong vibrations at 1165, 1288 (or 1284 for **B**), 1311, and 1505 cm^{-1}. These bands correspond to the following vibrational modes; CH_3 rocking, C–O stretching, C–H in-plane bending, and C=C ring stretching, respectively [51]. Reactant **A** has two additional bands at 1196(w) cm^{-1} and 1439(s) cm^{-1} which correspond to C–H in-plane bending modes and C=C ring stretching, respectively [51]. Meanwhile, intermediate **B** has four distinct bands at 1371(m), 1395(w), 1428(br,w) and 1475(br,w) cm^{-1}. These bands can be assigned to the CH_3 symmetric deformation, CH_2 wagging modes, CH_3 deformation and CH_2 scissoring modes in the ethyl group, respectively. These vibrational modes were inferred from the corresponding vibrational modes observed in ethyl benzoate [52]. It should be noted that the molecular vibrations described are primarily due to the functional groups mentioned, but these vibrations can also include other coupled motions in the molecule.

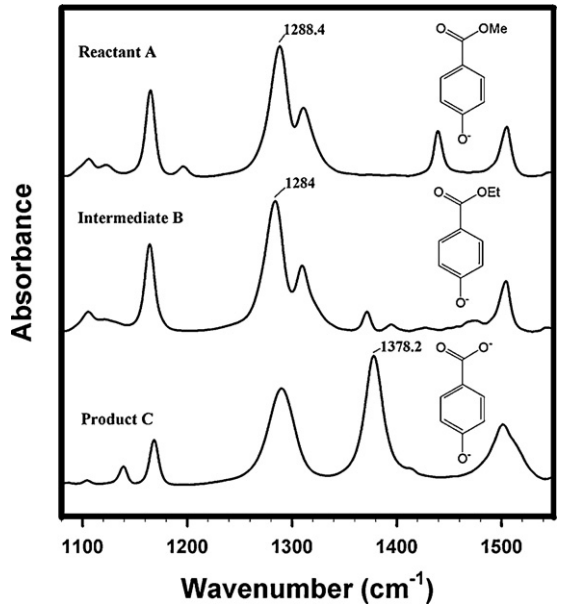

Fig. 2. BTEM pure component spectra of reactant **A** (deprotonation of MP), intermediate **B** (deprotonation of EP) and product **C**, obtained from data measured at 86% (v/v) water–ethanol solvent mixture i.e. Exp Run {1–7}.

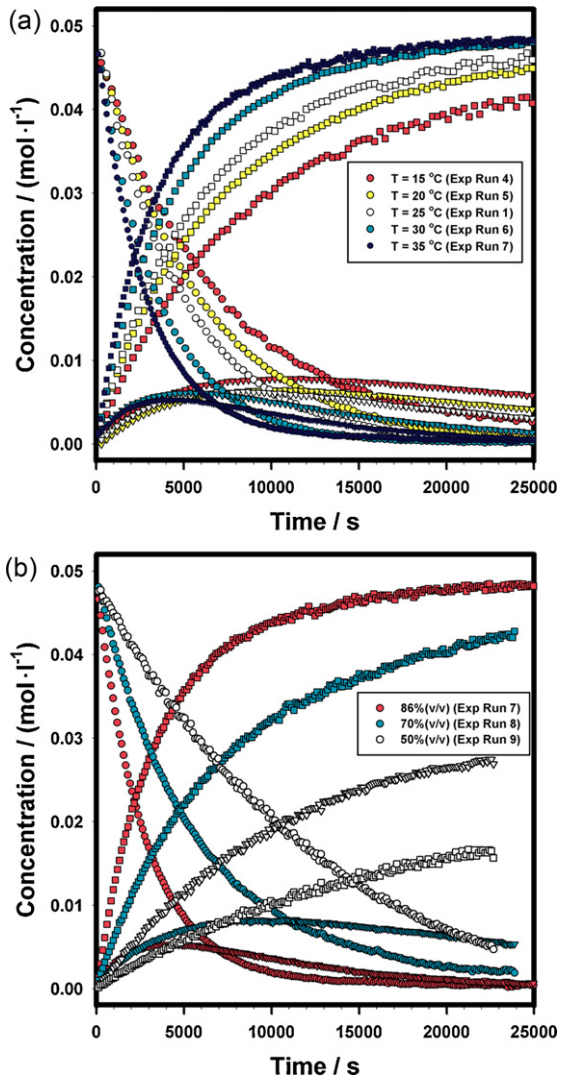

Fig. 3. (a) The effect of temperature and (b) the effect of solvent compositions on the transformation rates of the reactant (●), intermediate (▼) and product (■).

The pure component spectrum of product **C** is very different from those of reactant **A** and intermediate **B**. The spectrum of product **C** shows vibrational bands at 1104(w), 1139(m), 1168(m), 1290(s), 1378(vs), 1414 (w), and 1501(s) cm^{-1}. The vibrational bands at 1104, 1139, 1168, 1414 and 1501 cm^{-1} are associated with the aromatic ring vibrational modes [53]. Meanwhile, the bands at

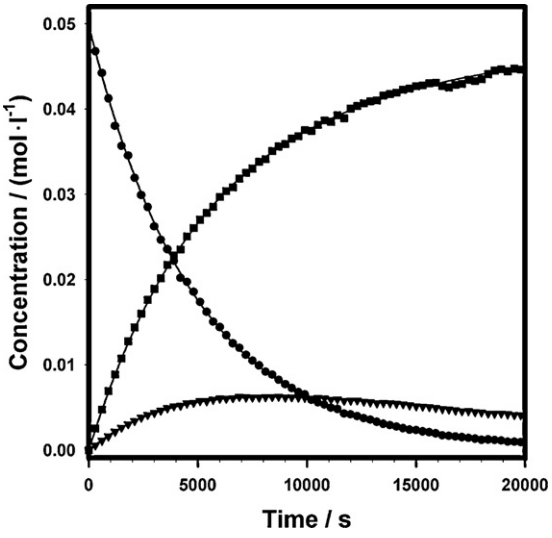

Fig. 4. Concentration profiles of the reactant (●), intermediate (▼) and product (■) from Exp Run 1. Solid lines represent the calculated concentrations derived from the kinetic models.

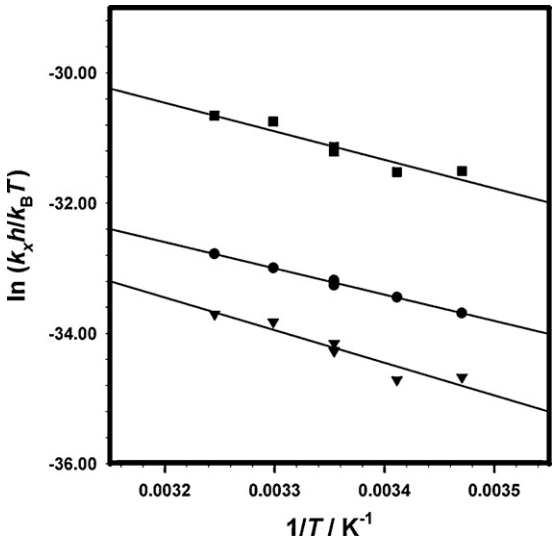

Fig. 5. Effect of temperature on the second-order rate constants k_{x1} (●), k_{x2} (▼) and k_{x3} (■) for 86% (v/v) water–ethanol mixtures.

1290 and 1378 cm^{-1} should correspond to the stretching of C–O^- and the symmetric stretching of COO^-, respectively.

Having obtained the pure component spectra of the three reactive species, the corresponding concentrations can be subsequently determined (see the numerical procedure in Section 3.2). The concentration profiles are shown at various temperatures (Exp Run 1–5) in Fig. 3(a) and various solvent compositions in Fig. 3(b). More detailed discussion concerning the effect of temperature and solvent compositions to the transformation rate are provided in the later section.

4.2. Kinetic analysis

The concentrations obtained from the spectroscopic analysis were subsequently used to evaluate the kinetic rate constants. Using the numerical procedure given in Section 3.3, the concentration profiles of the reactant, intermediate and product were generated from the proposed kinetic model equations. Good agreements between the measured and the calculated concentrations were observed in all experimental runs. The consistency between the measured and the calculated concentrations obtained from Exp Run 1 is shown in Fig. 4. This consistency indicates that the present complex triangular reaction system can be satisfactorily described by the kinetic model in Eqs. (9)–(12).

The kinetic analysis resulted in the optimized values for the three kinetic rate constants k_1, k_2 and k_3. The determined rate constants for all experimental runs are summarized in Table 2.

Table 2 shows that good reproducibility of rate constants can be achieved from the replicate measurements (Exp Runs 1–3). These reproducibility measurements are useful to show the consistency of the on-line spectroscopy measurements but also useful for estimating the uncertainties for the rate constants determined from the present measurements. The approximate uncertainty for the rate constants k_1, k_2 and k_3 are circa 4%, 6.5% and 0.4%, respectively.

In the triangular Scheme 1, there are 2 pathways for the synthesis of the final product **C** (sodium paraben). These are (1) the direct hydrolysis of **A**, and (2) the indirect formation via ethanolysis followed by hydrolysis. Integration of the term $k_1 C_{\mathbf{A}} C_{OH^-}$ over time provides the total concentration of product **C** formed via the direct synthetic route. For example, the analysis performed at 86% (v/v) water–ethanol at 35 °C, shows that circa 80% of the final product arises from this direct pathway. However, when the reaction was performed at 50% (v/v) water–ethanol at 35 °C, the indirect pathway is dominant and this pathway contributes circa 67% of the total product.

4.3. Effects of temperature

The effects of temperature on rate constants k_1, k_2 and k_3 can be seen in Table 2. All rate constants are consistently increasing with temperature. A further analysis of the effect of temperature on the reaction rate can be performed according to the Eyring equation in order to evaluate the enthalpy of activations ($\Delta H^{\ddagger}$) and the entropy of activation ($\Delta S^{\ddagger}$). Accordingly, the molar based rate constants k_i were first transformed to mole fraction based rate constants k_{xi} [54]. The linear plot of $\ln k_{xi}h/k_BT$ versus $1/T$ can be made and the results are shown in Fig. 5. The corresponding slopes and intercepts of this linear plot provide values for the enthalpy of activations ($\Delta H^{\ddagger}$) and the entropy of activation ($\Delta S^{\ddagger}$). The determined enthalpy of activations ($\Delta H^{\ddagger}$) were 33.5 kJ mol^{-1}, 41.6 kJ mol^{-1} and 36.5 kJ mol^{-1} and the determined entropy of activation ($\Delta S^{\ddagger}$) were −163.7 J mol^{-1} K^{-1}, −144.9 J mol^{-1} K^{-1} and

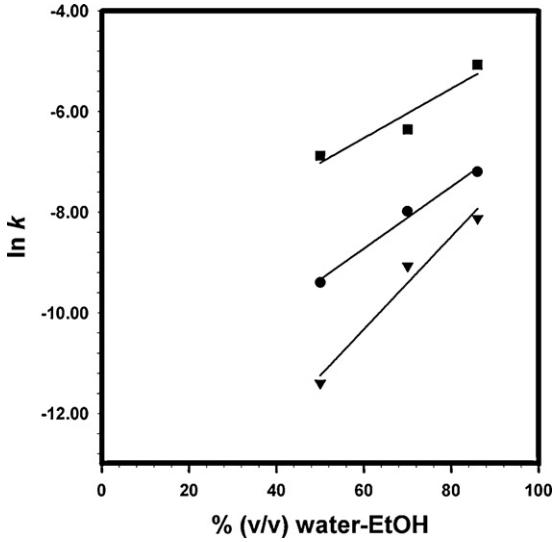

Fig. 6. Effect of solvent mixture on the second-order rate constants k_1 (●), k_2 (▼) and k_3 (■) at temperature 35 °C.

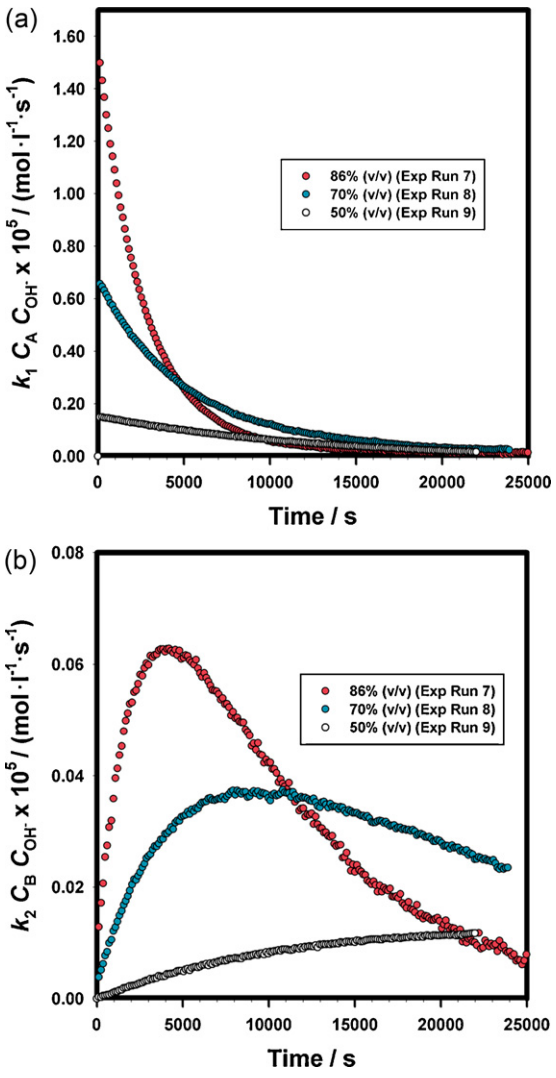

Fig. 7. Effect of the solvent mixture on the transformation rates of hydrolysis reactions of (a) reactant **A** and (b) intermediate **B**.

$-136.4\,J\,mol^{-1}\,K^{-1}$. These values correspond to the hydrolysis reaction of the deprotonated MP, the hydrolysis reaction of the deprotonated EP, and the ethanolysis of the deprotonated MP, respectively. Both the sign and magnitude of the entropy of the activations are consistent with the associative nature of the elementary steps involved in the hydrolysis and ethanolysis reactions. In particular, the negative entropies of activation are indicative of a bimolecular reaction.

4.4. Effects of solvent mixture

The effect of solvent mixtures on the kinetic rate constants is shown in Fig. 6 for those experimental runs carried out at $T = 35\,^{\circ}C$. The plot shows that the solvent mixture composition has a considerable impact on the reaction rate constants. The rate constants for both hydrolysis and ethanolysis reactions decrease with increasing ethanol concentration.

The composition of the water–ethanol solvent mixtures influenced both the rates of hydrolysis and alcoholysis. An increased concentration of ethanol in the alkaline water–ethanol solvent mixture will (i) reduce the concentration of hydroxide ion, (ii) increase the concentration of ion ethoxide and (iii) stabilize the hydrophobic ions/molecules [55,56], in this particular case the reactant **A** (deprotonated MP) and the intermediate **B** (deprotonated EP). It

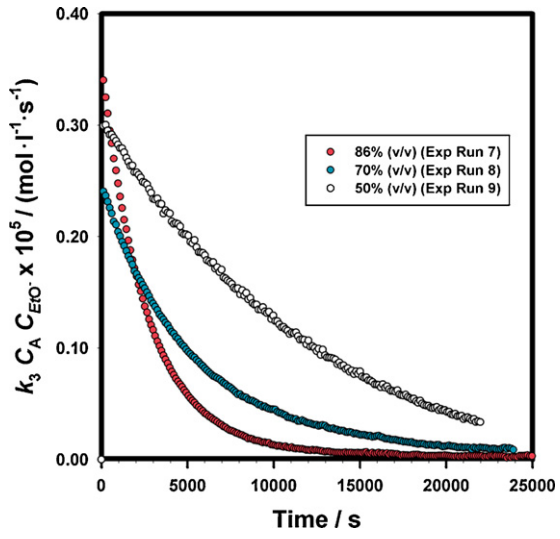

Fig. 8. Effect of the solvent mixture on the initial transformation rates of ethanolysis reactions of reactant **A**.

can be expected that the stabilization effect on the later compound is greater since the deprotonated EP is more hydrophobic than the deprotonated MP.

Since a lower concentration of hydroxide ion is available for the reaction and both reactant **A** and intermediate **B** are more stable with the presence of ethanol, the transformation rates of hydrolysis reactions should decrease. The rates of hydrolysis reactions of reactant **A** and intermediate **B** performed at different solvent mixture are shown in Fig. 7(a) and (b), respectively. The results show that initial rates (i.e. first 2000 s) for both hydrolysis reactions decreases with the increase of ethanol concentration.

With respect to the ethanolysis reaction, an increased initial concentration of ethanol provides a higher concentration of ethoxide ion as well as stabilizes the reactant **A**. These two factors cause two competing effects on the net reaction rate. The former effect facilitates increasing rate for the reaction and the latter tends to decrease the rate of reaction. As seen in Fig. 8, these competing effects lead to high then low then high initial transformation rate of ethanolysis (initial rates are $0.34 \times 10^{-5}\,mol\,l^{-1}\,s^{-1}$ at 86%, $0.24 \times 10^{-5}\,mol\,l^{-1}\,s^{-1}$ at 70%, and $0.30 \times 10^{-5}\,mol\,l^{-1}\,s^{-1}$ at 50%). The decreasing rate observed for 86–70% (v/v) water–EtOH solvent mixtures suggests that the stabilization effect on the reactant **A** is a dominant factor. Increasing the ethanol concentration further (i.e. 50% (v/v) water–EtOH) causes an increase of net reaction rate due to the increase of ethoxide ion concentration.

5. Conclusions

This study demonstrates the utility of on-line transmission FTIR and advanced signal processing method BTEM to monitor and investigate the kinetics of a complex triangular reaction starting from methyl 4-hydrozybenzoate performed in alkaline water–ethanol solvent media. This combined analytical tool has been shown to be robust and reliable to identify and to obtain the pure component spectra of each reactive species (including the presence of intermediate) involved in the reactions. These pure component spectra are used subsequently to obtain the concentration profiles and to evaluate the kinetic rate constants.

The kinetic study on the present triangular complex reaction reveals that both temperature and solvent mixture composition can greatly affect the individual rates of both hydrolysis and ethanolysis reactions. The analysis of the temperature effect on the kinetic rate constants confirms that bimolecular reactions involving an asso-

ciative nature occur in both types of reactions. The effect of solvent mixture on the transformation rates shows that the increase of ethanol concentration decreases the hydrolysis reaction. The effect of solvent mixture on the net rate of ethanolysis reaction is more complex and influenced by at least two competing factors, namely the concentration of ethoxide ion in the solution and the stabilization effect on the reactant. The effect of solvent mixture is indeed crucial and determines the dominant pathway in the formation of the final product (either through direct hydrolysis or indirect formation via ethanolysis followed by hydrolysis) in the present triangular reaction system.

Acknowledgements

This work was supported by Agency for Science, Technology and Research (A*STAR), Singapore. We also wish to thank Prof Paul Sharratt for helpful discussions.

References

[1] C.J. Li, T.H. Chan, Comprehensive Organic Reactions in Aqueous Media, second ed., John Wiley & Sons, Hoboken, NJ, 2007.
[2] P. Knochel (Ed.), Modern Solvent in Organic Synthesis, Topics in Current Chemistry, vol. 206, Springer, Berlin, 1999.
[3] D.J. Adams, P.J. Dyson, S.J. Tavener, Chemistry in Alternative Reaction Media, J. Wiley, Chichester, West Sussex, England/Hoboken, NJ, 2004.
[4] B. Cornils, W.A. Herrmann, Aqueous-phase Organometallic Catalysis: Concepts and Applications, second ed., Wiley-VCH, Weinheim, 1998.
[5] F. Joó, Aqueous Organometallic Catalysis, Kluwer Academic Publishers, Dordrecht, Boston, 2001.
[6] B. Heaton (Ed.), Mechanisms in Homogeneous Catalysis: A Spectroscopic Approach, Wiley-VCH, Weinheim, 2005.
[7] W.R. Moser, A.W. Wang, N.K. Kildahl, J. Am. Chem. Soc. 110 (1988) 2816–2820.
[8] W.R. Moser, B.J. Marshik-Guerts, S.J. Okrasinski, J. Mol. Catal. A: Chem. 143 (1999) 57–69.
[9] A. Haynes, P.M. Maitlis, G.E. Morris, G.J. Sunley, H. Adams, P.W. Badger, C.M. Bowers, D.B. Cook, P.I.P. Elliott, T. Ghaffar, H. Green, T.R. Griffin, M. Payne, J.M. Pearson, M.J. Taylor, P.W. Vickers, R.J. Watt, J. Am. Chem. Soc. 126 (2004) 2847–2861.
[10] G. Bor, Spectrochim. Acta 19 (1963) 2065–2073.
[11] K. Noack, Spectrochim. Acta 19 (1963) 1925–1931.
[12] H.B. Tinker, D.E. Morris, Rev. Sci. Instrum. 43 (1972) 1024–1026.
[13] G. Bor, U.K. Dietler, P. Pino, J. Organomet. Chem. 754 (1978) 301–315.
[14] M.B. Simpson, M. Poliakoff, J.J. Turner, W.B. Maier, J.G. McLaughlin, J. Chem. Soc. Chem. Commun. (1983) 1355–1357.
[15] W.B. Maier, M. Poliakoff, M.B. Simpson, J.J. Turner, J. Mol. Struct. 80 (1982) 83–86.
[16] R. Whyman, J. Organomet. Chem. 66 (1974) C23–C25.
[17] R. Whyman, J. Organomet. Chem. 81 (1974) 97–106.
[18] M. van Boven, N. Alemdaroglu, J.M.L. Penninger, Ind. Eng. Chem. Prod. Res. Dev. 14 (1975) 259–264.
[19] D. Forster, J. Am. Chem. Soc. 98 (1976) 846–848.
[20] B.E. Mann, B.L. Shaw, R.E. Stainbank, J. Chem. Soc. Chem. Commun. (1972) 151–152.
[21] B.T. Heaton, J. Jonas, T. Eguchi, G.A. Hoffmann, J. Chem. Soc. Chem. Commun. (1981) 331–332.
[22] B.T. Heaton, L. Strona, J. Jonas, T. Eguchi, G.A. Hoffmann, J. Chem. Soc. Dalton Trans. (1982) 1159–1164.
[23] B.T. Heaton, D.J.A. McCaffrey, J. Chem. Soc. Dalton Trans. (1979) 1078–1083.
[24] J.M. Brown, A.G. Kent, J. Chem. Soc. Chem. Commun. (1982) 723–725.
[25] E. Venardou, E. Garcia-Verdugo, S.J. Barlow, Y.E. Gorbaty, M. Poliakoff, Vib. Spectrosc. 35 (2004) 103–109.
[26] S. Guo, Z. Du, S. Zhang, D. Li, Z. Li, Y. Deng, Green Chem. 8 (2006) 296–300.
[27] N.E. Leadbeater, R.J. Smith, Org. Lett. 8 (2006) 4589–4591.
[28] J.R. Schmink, J.L. Holcomb, N.E. Leadbeater, Chem. Eur. J. 14 (2008) 9943–9950.
[29] E. Widjaja, C.Z. Li, M. Garland, Organometallics 21 (2002) 1991–1997.
[30] W. Chew, E. Widjaja, M. Garland, Organometallics 21 (2002) 1982–1990.
[31] E. Widjaja, C.Z. Li, W. Chew, M. Garland, Anal. Chem. 75 (2003) 4499–4507.
[32] C.Z. Li, E. Widjaja, M. Garland, J. Am. Chem. Soc. 125 (2003) 5540–5548.
[33] C.Z. Li, E. Widjaja, M. Garland, J. Catal. 213 (2003) 126–134.
[34] A.D. Allian, M. Garland, Dalton Trans. (2005) 1957–1965.
[35] R. Pacheco, A. Karmali, M.L.M. Serralheiro, P.I. Haris, Anal. Biochem. 346 (2005) 49–58.
[36] M. Tjahjono, H. Chong, E. Widjaja, K. Sa-ei, M. Garland, Talanta 79 (2009) 856–862.
[37] M. Tjahjono, E. Widjaja, M. Garland, ChemPhysChem 10 (2009) 1274–1283.
[38] M. Hancer, R.P. Sperline, J.D. Miller, Appl. Spectrosc. 54 (2000) 138–143.
[39] K. Yamamoto, H. Ishida, Vib. Spectrosc. 8 (1994) 1–36.
[40] A.G. Fredrickson, Chem. Eng. Sci. 21 (1966) 687–691.
[41] J. Wei, C.D. Prater, Adv. Catal. 13 (1962) 203–392.
[42] A.T. Aguayo, J.M. Arandes, M. Olazar, J. Bilbao, Ind. Eng. Chem. Res. 29 (1990) 1172–1178.
[43] K. Klier, V. Chatikavanij, R.G. Herman, G.W. Simmons, J. Catal. 74 (1982) 343–360.
[44] G. Liu, D. Willcox, M. Garland, H.H. Kung, J. Catal. 96 (1985) 251–260.
[45] V.B. Sunderland, D.W. Watts, Int. J. Pharm. 27 (1985) 1–15.
[46] R.C. Rowe, P.J. Sheskey, S.C. Owen, Handbook of Pharmaceutical Excipients, American Pharmacists Association, Washington, 2006.
[47] L. Chen, M. Garland, Appl. Spectrosc. 56 (2002) 1422–1428.
[48] C.A. Lieber, A. Mahadevan-Jansen, Appl. Spectrosc. 57 (2003) 1363–1367.
[49] F.F. Caldin, G. Long, J. Chem. Soc. (1954) 3737–3742.
[50] J. Murto, Ann. Acad. Sci. Fenn. Ser. A2 117 (1962) 1–84.
[51] D. Sajan, H. Joe, V.S. Jayakumar, J. Zaleski, J. Mol. Struct. 785 (2006) 43–53.
[52] M. Ystenes, E. Rytter, Spectrochim. Acta A 48 (1992) 543–555.
[53] B. Dasiewicz, L. Fuks, W. Lewandowski, J. Mol. Struct. 565–566 (2001) 1–6.
[54] K.A. Connors, Chemical Kinetics: The Study of Reaction Rates in Solution, VCH, New York, 1990 (Chapter 6).
[55] M.J. Blandamer, J. Burgess, Chem. Soc. Rev. 4 (1975) 55–75.
[56] N.J. Buurma, L. Pastorello, M.J. Blandamer, J.B.F.N. Engberts, J. Am. Chem. Soc. 123 (2001) 11848–11853.